

## Effects of annulus gap on flow and temperature field in electromagnetic direct chill casting process

TANG Meng-ou, XU Jun, ZHANG Zhi-feng, BAI Yue-long

General Research Institute for Nonferrous Metals, Beijing 100088, China

Received 13 May 2010; accepted 20 November 2010

**Abstract:** A comprehensive mathematical model of annulus-electromagnetic direct chill (A-EMDC) casting of A357 aluminum alloy was established with corresponding experimental verification. The model was based on a combination of the commercial finite element package ANSYS and the commercial finite volume package FLUENT. The effects of structural parameters on fluid flow, temperature field and solidification during A-EMDC process were investigated numerically. The results show that structural parameters such as annulus gap width, annulus gap position, and centre pipe length influence the flow and temperature fields. The smaller the annulus gap width is, the more uniform the temperature is, and the smaller the temperature gradient is. With increasing the centre pipe length, the circular flow would decrease due to the dislocation of centre pipe. Specially, when the annulus gap is located at periphery of the billet, the temperature gradient of the longitudinal direction in the solidification region falls evidently.

**Key words:** electromagnetic stirring; continuous casting; coupled modeling; annulus gap

### 1 Introduction

Direct chill casting with electromagnetic stirring (DCC-EMS) possesses advantages of internal structures refinement, reduction of segregation and cavity shrinkage[1–3]. Presently, DCC-EMS technology has been a main method for producing the semi-solid billets on a commercial scale due to its non-pollution, easy process control and continuous production[4–6]. However, it has some shortcomings. In the stirring process, the stirring force exerted in the slurry is different between the surface layer and inner of the slurry because of the skin effect resulting from electromagnetic induction; and the force exerted in the surface layer is much larger than that in the inner of the slurry. Therefore, the skin effect restricts the casting diameter. In order to avoid this problem, combining hot-top continuous casting technology and the annulus electromagnetic stirring (A-EMS) process[7–8], an advanced semi-solid metal processing technology, namely, the annulus electromagnetic direct chill (A-EMDC) casting process has been developed by the authors[9]. Figure 1 shows a sketch of the A-EMDC process. The annulus gap is advantageous to increasing circular flow, reducing the

temperature gradient as well as shallowing liquid sump depth in the A-EMDC. The microstructure obtained by the A-EMDC is globular or rosette-like, and the microstructure in the billet is homogeneous.

In the present study, a comprehensive mathematic model was developed to describe the interaction of the multiple physics fields (electromagnetic field, fluid flow, heat transfer and solidification) during the A-EMDC

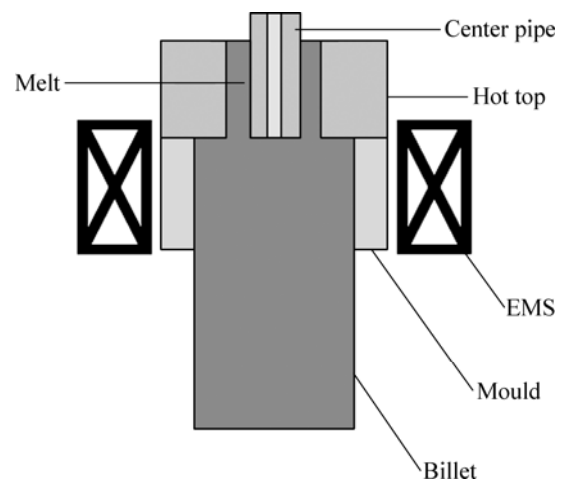


**Fig.1** Schematic diagram of A-EMDC casting apparatus

process. Effects of A-EMDC structural parameters such as annulus gap width, annulus gap position, and centre pipe length on macroscopic transport phenomena during solidification were investigated with corresponding experimental verification. The knowledge gained from this model would be used to develop guidance for the design and the operation of A-EMDC, and to understand the phenomenon occurring during A-EMDC casting process.

## 2 Experimental

A357 aluminum alloy billets with diameter of 90 mm were cast by A-EMDC process at melt temperature of 973 K, and the casting speed of 3 mm/s. The electromagnetic field was applied by a 175 turns water cooling copper coil surrounding the mould made of duraluminium. The current frequency in the coil was fixed at 25 Hz and the current intensity was 50 A during the A-EMDC process. The height of hot-top was 100 mm.

The NETZSCH STA409 PC machine was utilized to investigate the specific heat capacity–temperature curves of A357 alloy. When there is no aluminum in the continuous casting machine, the magnetic flux density was measured with and without centre pipe in longitudinal and transverse directions. The schematic diagram of temperature measurement and the location of thermocouples are shown in Fig.2. Line 1–1 is parallel to  $X$ -axis, 8 mm away from the origin of coordinate. The grid origin stands at the center of the mould. Line 2–2 is the centerline of the annulus gap. In Fig.2(a), the diameter of mould is 90 mm, the diameter of hot-top is 65 mm and the gap width is 20 mm. In Fig.2(b), the diameter of mould is 90 mm, the diameter of hot-top is 65 mm and there is no centre pipe. CT3 teslameter made by Shanghai Fourth Electric Meter Factory was utilized to measure the magnetic flux density. In order to study the effects of annulus gap on temperature field, temperature measurement was performed during casting.

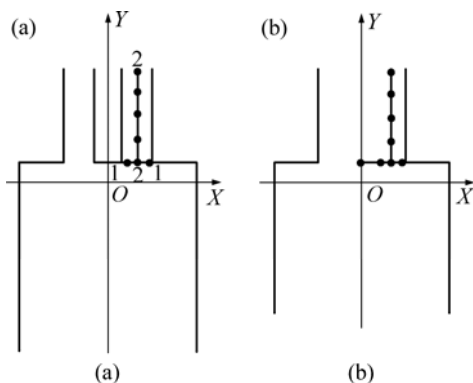


**Fig.2** Schematic diagram of magnetic flux density measurement: (a) A-EMDC; (b) DCC-EMS

After some distance, a nearly steady-state regime was established for the thermal field. A K-thermocouple was inserted in the billet at the middle of annulus gap as line 2–2 in Fig.2(a). Another K-thermocouple was inserted in the billet at the middle of hot-top as  $Y$ -axis in Fig.2(b). The thermocouple moved with the billet and was eventually frozen into solid metal. Then the temperature curve of these lines in the billet can be obtained.

## 3 Simulation description

### 3.1 Numerical procedures

The governing equations of electromagnetic field and others fields were solved by using the commercial software ANSYS and FLUENT, respectively. The time average electromagnetic volume force density was added to the conservation equation of momentum as the momentum source term during solving flow field. During calculation procedure of electromagnetic field based on ANSYS, a magnetic vector potential method was used. Furthermore, when the other fields were calculated based on FLUENT, pressure–velocity coupling algorithm is SIMPLE algorithm and the difference schemes are the first order upwind schemes in FLUENT[10–12].

### 3.2 Basic assumptions

A series of complicated phenomena take place in the continuous casting process such as flow, heat transfer, solidification, solute segregation, and electromagnetic induction in which flow and solidification are the basic phenomena. Taking all these phenomena into account in the model is impossible. By appropriately simplifying the model, the present study puts the emphasis upon the magnetic induction and heat transfer in mold cavity, especially on the thermal field. The assumptions in the model are given as follows:

- 1) The molten aluminum flow in the mold is a steady state, and incompressible viscosity flow process;
- 2) Joule heat, the calculation of the solute field and the taper of the mold walls are not considered in this model;
- 3) All materials in the model are regarded as homogeneous phase media;
- 4) The time-averaged force substitutes the time-varying force;
- 5) The displacement current  $\partial D/\partial t$  is neglected;
- 6) The variety of the fluid field has little effect on the distribution of the magnetic field.

### 3.3 Determination of boundary and material properties

In the calculation, the relative permeabilities of air, copper and aluminum are 1. The relative permeability of

silicon steel is 2 000. The electrical resistivities of duraluminium mould and the melt are  $3.1 \times 10^{-7}$  and  $2.1 \times 10^{-7} \Omega \cdot \text{m}$ , respectively. The viscosity of the aluminum is  $2.7 \times 10^{-3} \text{ Pa} \cdot \text{s}$ , the density is  $2\,700 \text{ kg/m}^3$ , and the thermal conductivity is  $155 \text{ W/(m} \cdot \text{K)}$ . In the course of aluminum solidification, the phase latent heat release raises the liquid temperature. The method of equivalent specific heat capacity is considered. Figure 3 shows the specific heat capacity—temperature curves of A357 alloy. The conclusion can be drawn from specific heat capacity—temperature curve that the equilibrium solidus temperature, liquidus temperature and solidification temperature range of the alloy are 808, 882 and 74 K, respectively.

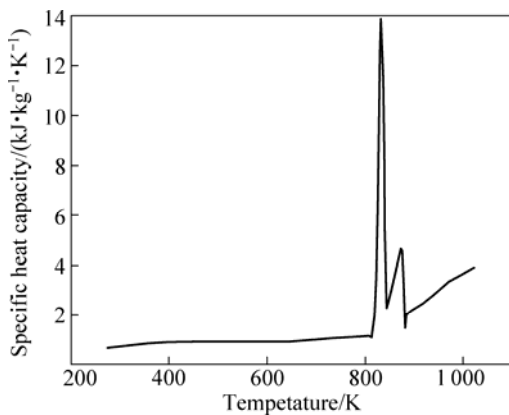


Fig.3 Specific heat capacity—temperature curve of A357 alloy

In terms of the thermal boundary condition, the heat transfer coefficient at annulus graphite is  $2\,000 \text{ W/(m}^2 \cdot \text{K)}$ . The secondary cooling boundary is divided into two zones, namely, impingement zone and streaming zone. There are also Cauchy-type boundary conditions, which are formulated according to Eq.(1) and Eq.(2), respectively[13].

$$h = Q^{0.33} [352(T_s + T_w) - 167\,000] + 20.8(T_s - 273)^3 \quad (1)$$

where  $h$  is the heat transfer coefficient at impingement zone;  $T_s$  is the ingot surface temperature;  $T_w$  is the saturation temperature of water;  $Q$  is the cooling water flow rate per unit width of film.

$$h_c = (-1.67 \times 10^5 + 704\bar{T})Q^{1/3} \quad (2)$$

where  $h_c$  is the heat transfer coefficient at streaming zone;  $\bar{T}$  is the average of bulk fluid temperature and wall temperature;  $Q$  is the cooling water flow rate per unit width of film.

## 4 Results and discussion

### 4.1 Comparison between calculated results and experimental results

The model predictions with the data measured from

the teslameter were compared, as shown in Fig.4. There are the similar distributions for all apparatus. For example, the magnetic flux density, with the maximum near the mould, falls gradually toward the center in transverse direction; and with the maximum near the magnetic yoke, falls gradually toward the periphery in longitudinal direction. The agreement between the model prediction and the measurement is good at the various locations examined in the mould without aluminum, indicating that the magnetic model can be used to develop guidance for the design of electromagnetic stirring apparatus. On the other hand, Figure 4 also indicates that the annulus gap avoids the part of low magnetic flux density.

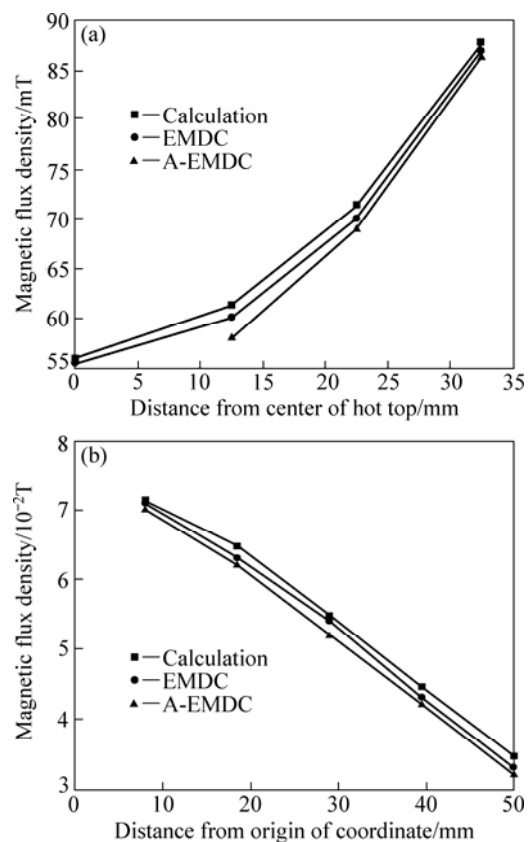
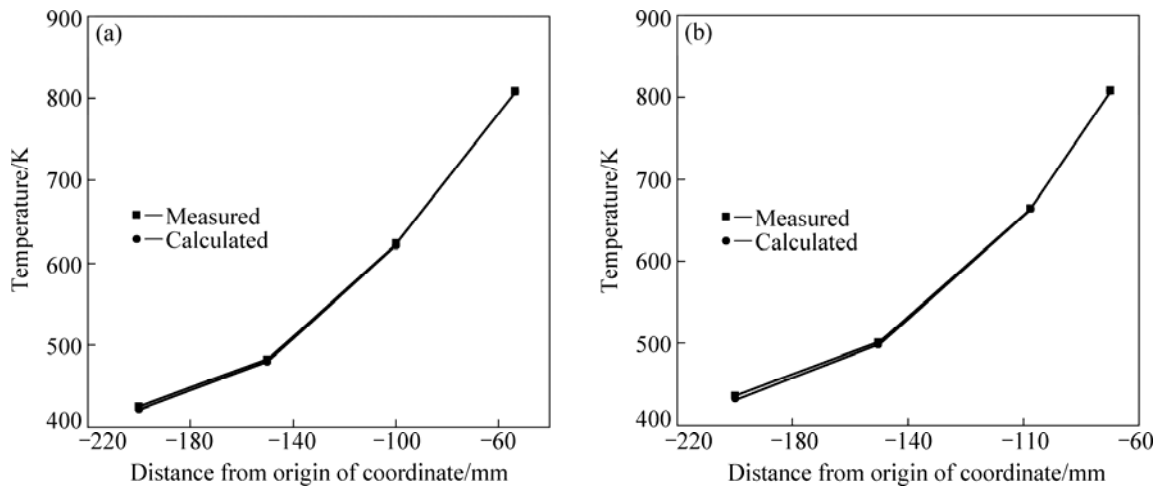


Fig.4 Comparison of measured and model predicted magnetic flux densities in different directions ( $I=50 \text{ A}$ ,  $f=25 \text{ Hz}$ ): (a) Transverse direction ( $y=8 \text{ mm}$ ); (b) Longitudinal direction ( $x=55 \text{ mm}$ )

Figure 5 shows the comparison of the measured and the calculated temperatures at the middle of hot-top or annulus gap during DCC-EMS and A-EMDC process, respectively. It is indicated that there is a good agreement between the calculated results and the measured results regardless of the DCC-EMS and A-EMDC processes.

### 4.2 Effect of annulus gap width on flow and temperature field

Figure 6 gives the velocity distributions within the



**Fig.5** Comparison of measured and model predicted temperatures for different apparatus ( $I=50$  A,  $f=25$  Hz): (a) A-EMDC ( $x=55$  mm); (b) DCC-EMS ( $x=0$  mm)

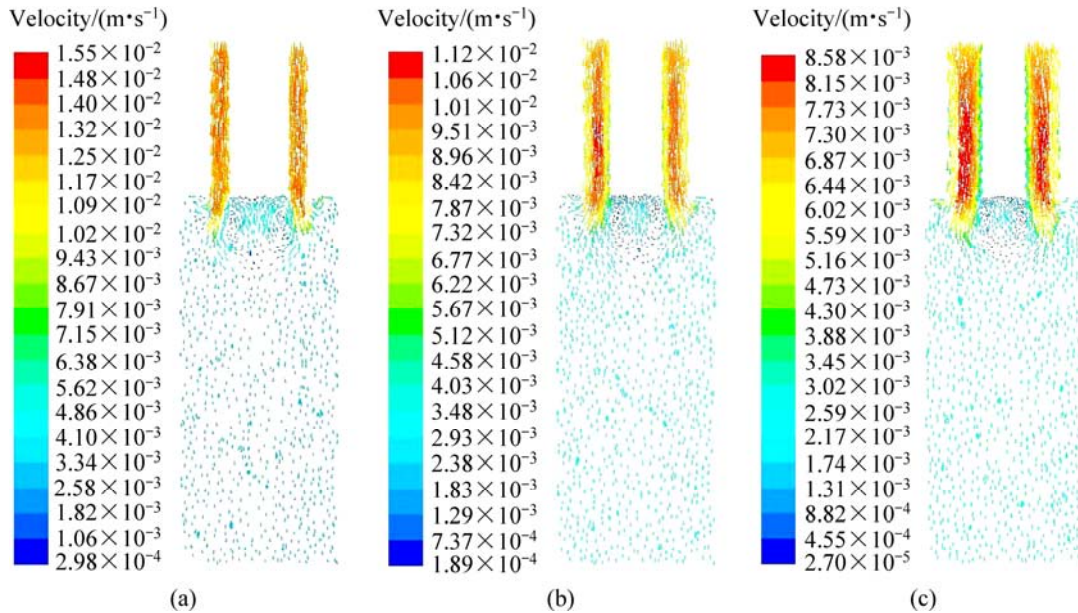


**Fig.6** Effect of annulus gap width on flow field: (a) 10 mm; (b) 15 mm; (c) 20 mm

melt with the annulus gap width changing from 10 to 20 mm, and locating at the middle of radius. It can be seen that there are the similar distributions for all width, i.e. two vortices occur within the mould under the centre pipe, which could reduce the temperature gradient effectively in virtue of liquid convection between the center and the skin areas. From Fig.6, with increasing the annulus gap width, the vortices would decrease, and move somewhat upward.

The annulus gap is advantageous to increasing shear rate. According to the calculation method applied by SPENCER and FLEMINGS[14], the average shear rate  $\gamma$  may be calculated by:

$$\gamma = \frac{2Rr}{R^2 - r^2} \cdot \frac{2\pi n}{60} \quad (3)$$

where  $\gamma$  is the average shear rate;  $R$  is the inner radius of hot-top;  $r$  is the outer radius of the centre pipe;  $n$  is the rotation speed of the magnetic field and is determined by equation:

$$n = \frac{60f}{p} \quad (4)$$

where  $p$  is the pole number; and  $f$  is the frequency.

In this work, the pole number  $p$  is 3, the frequency is 25 Hz and the annulus gap width is 10 mm. So the average shear rate exerted in the slurry is calculated to be  $111.93 \text{ s}^{-1}$ . Similarly, when the annulus gap widths are 15 mm and 20 mm, the average shear rates are  $69.77 \text{ s}^{-1}$  and  $47.24 \text{ s}^{-1}$ , respectively. That is to say, the shear rate increases with decreasing the annulus gap width when the casting velocity is zero. Accordingly, the scouring

effect of the vortices on the mushy region enhances, which is in favor of the grain refinement of the microstructure. But too narrow gap is not in favor of operating.

The temperature field varies with the change of flow pattern, as shown in Fig.7. Figure 7 indicates that there are similar shapes of isothermal lines after increasing gap width at casting velocity of 3 mm/s. But the isothermal line of the liquidus temperature would more even with decreasing gap width and the meniscus moves towards the lower part along the billet axis.

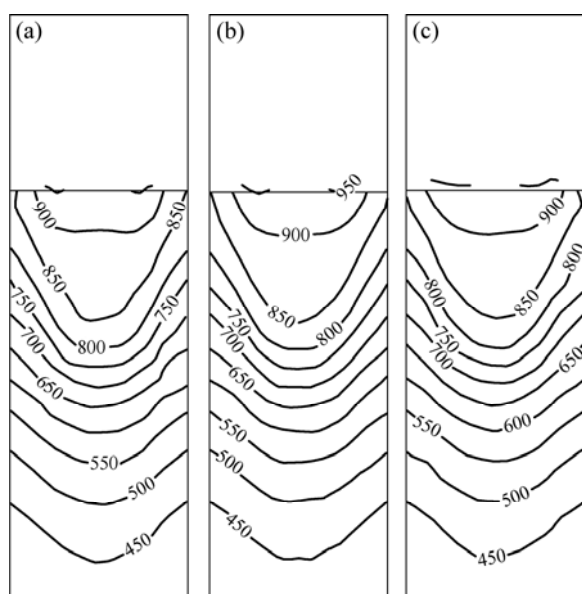


**Fig.7** Effect of annulus gap width on temperature field: (a) 10 mm; (b) 15 mm; (c) 20 mm

### 4.3 Effect of centre pipe length on flow and temperature field

Flow fields in the different length centre pipes are shown in Fig.8. It is found that the melt flows in the

same as those in Fig.6, that is, there is a pair of vortices in bulk liquid under the center pipe. Figure 8 shows that the fluid flow is axisymmetric, including axial flow and circular flow. Centre pipe length has no effect on the direction of the melt flow, as seen from the velocity vectors in Fig.8. The left is an anticlockwise vortex with a long elliptical shape, and the right is a clockwise vortex. It is found that with increasing the centre pipe length, the circular flow would decrease due to the dislocation of centre pipe.

As the foregoing statement, the temperature field varies with the change of flow pattern. It is obvious that the temperature gradient along the longitudinal direction in the solidification region falls, as shown in Fig.9(a). The circular flow is in virtue of liquid convection between the center and the skin areas. And the heat can be rejected effectively and quickly with circular flow. The axial flow is not effective and quick enough to reject heat, and the melt with higher temperature would gather in the center part. So enhancing circular flow is of key importance for realizing uniform temperature of bulk melt. As a result, not only the annulus gap was designed to avoid the part of low magnetic flux density, but also structural parameters such as annulus gap width, annulus gap position, and centre pipe length were investigated. That is to say, optimal designed configuration, i.e. the match of hot-top, mould, stirrer and centre pipe, is of key importance for realizing uniform temperature of bulk melt.

### 4.4 Effect of annulus gap position on flow and temperature field

Figure 10 shows the flow field of A357 alloy obtained at different annulus gap positions. In the preceding analyses of simulation results, it is assumed that annulus gap is located at the middle of radius. When the inner diameter of annulus gap is 0, the annulus gap at

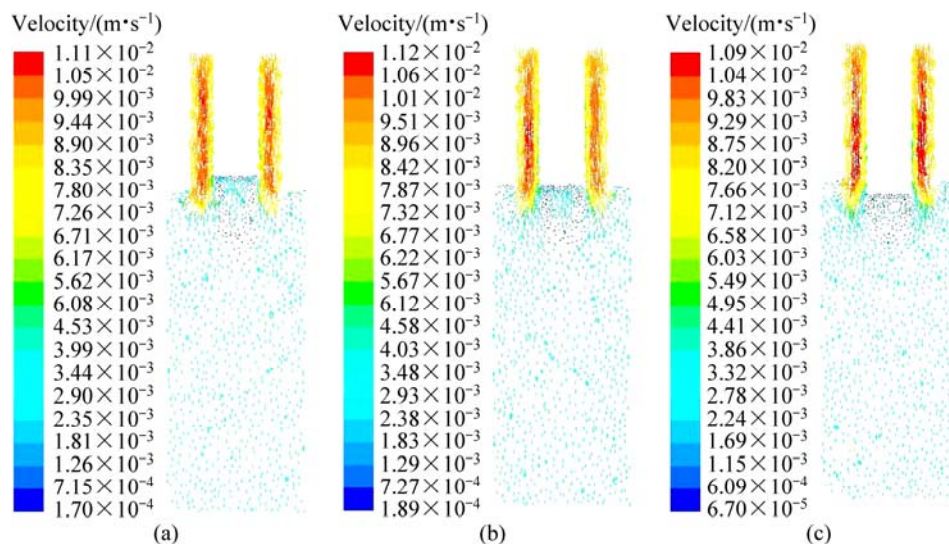


**Fig.8** Effect of centre pipe length on flow field: (a) 90 mm; (b) 100 mm; (c) 110 mm

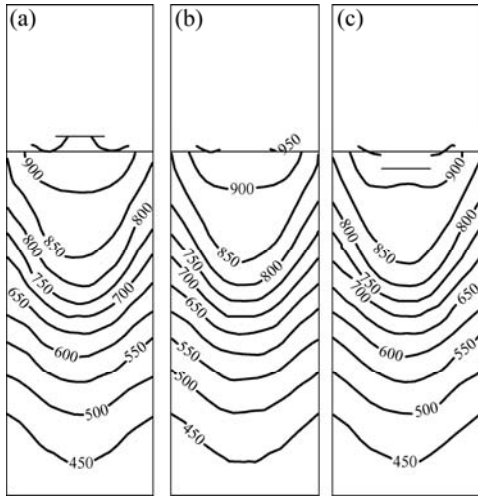


**Fig.9** Effect of centre pipe length on temperature field: (a) 90 mm; (b) 100 mm; (c) 110 mm

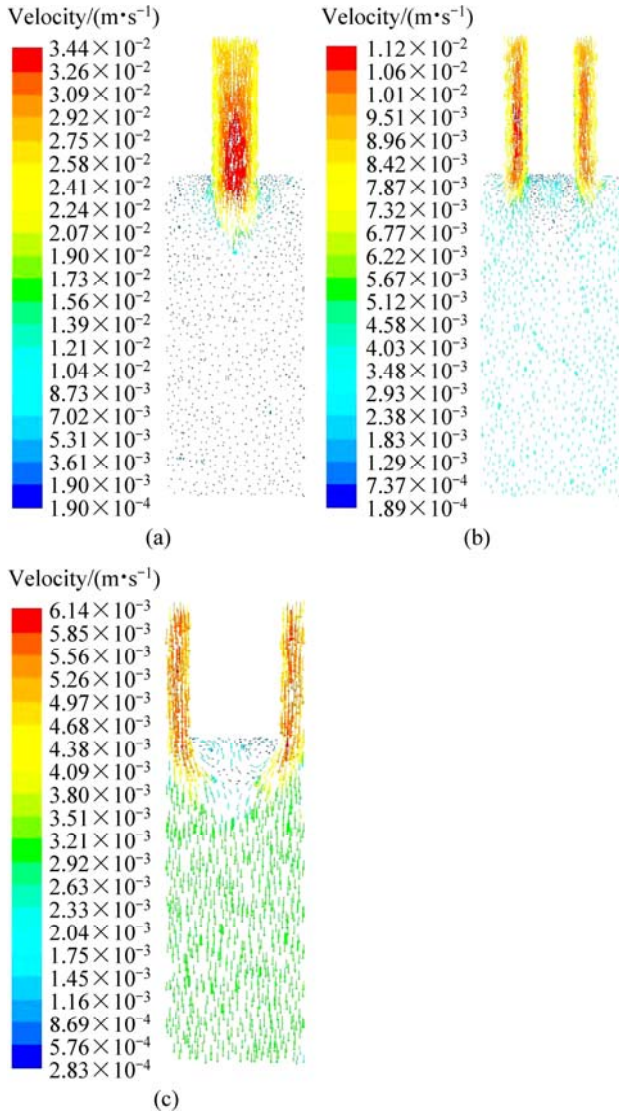


**Fig.10** Effect of annulus gap position on flow field: (a) Centre; (b) Middle; (c) Edge

width of 15 mm becomes a hot-top with diameter of 30 mm, as shown in Fig.10(a). The melt flows into the hot-top vertically. Therefore, the melt with higher temperature would gather in the center part, and the heat cannot be rejected effectively and quickly, so a deep liquid sump would present in the middle part of the billet, as shown in Fig.11(a). Figure 10(c) gives the velocity distribution within the melt when the width of annulus gap is 15 mm, locating at periphery of the billet. There are two vortices under the centre pipe, which are larger than those in Figs.10(a), (b).

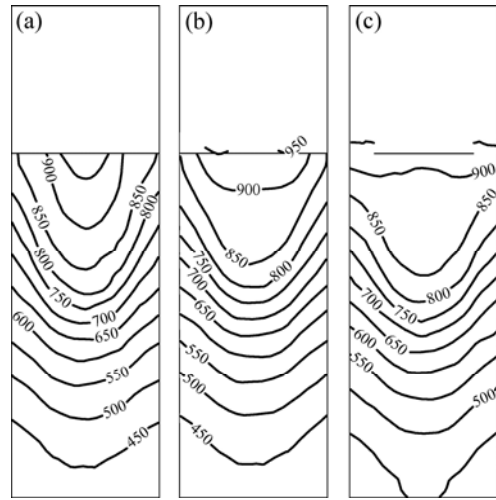


**Fig.11** Effect of annulus gap position on temperature field: (a) Centre; (b) Middle; (c) Edge

It is known that the density of the isothermal lines reflects the temperature gradient. It is obvious that the temperature gradient along the longitudinal direction in the solidification region falls and the depth of liquid sump shallows evidently in Fig.11(c). This means that there is a large mushy zone in Fig.11(c). Nucleation will occur in the entire volume of the liquid and each nucleus will survive. Many studies have already manifested that high grain density is beneficial to the spherical growth of primary phases[5, 15]. The probability of overlap of diffusion fields of the adjacent grains increases, which leads to decreasing concentration gradient in front of solid-liquid interface and increasing their interface stability. Under this situation, the growth will be limited and stable, and ideal globular microstructures can be obtained.

### 5 Conclusions

1) A numerical model for the coupled calculation of electromagnetic field, fluid flow, heat transfer and solidification during the A-EMDC processes is presented using software ANSYS and FLUENT. The numerical magnetic flux density and temperature are in good qualitative agreement with the measured results.

2) With increasing annulus gap width, the vortexes would decrease, and move somewhat upward. But too narrow gap is not in favor of operating. With increasing centre pipe depth, the circular flow would decrease due to the dislocation of centre pipe.

3) When annulus gap is at periphery of the billet, there are two large vortexes under the centre pipe. And the temperature gradient of the longitudinal direction in the solidification region falls and the depth of liquid sump shallows evidently.

## References

- [1] GETSELEV Z V. Casting in an electromagnetic mold [J]. Journal of Metals, 1971, 23(10): 38–43.
- [2] VIVES C, RICOU R. Experimental study of continuous electromagnetic casting of aluminum alloy [J]. Metallurgical Transactions B, 1985, 16(2): 377–384.
- [3] VIVES C. Electromagnetic refining of aluminum alloys by the CREM process. Part I: Working principle and metallurgical results [J]. Metallurgical Transactions B, 1989, 20(5): 623–629.
- [4] MIDSON S P. The commercial status of semi-solid casting in the USA [C]// Proceeding of the 4th International Conference on the Processing of Semi-Solid Alloys and Composite. Sheffield, 1996: 251–255.
- [5] FAN Z. Semi-solid metal processing [J]. International Materials Reviews, 2002, 47(2): 1–37.
- [6] LUO Shou-jing, KEUNG W C, KANG Yong-lin. Theory and application research development of semi-solid forming in China [J]. Transactions of Nonferrous Metals Society of China, 2010, 20(9): 1805–1814.
- [7] XU Jun, ZHANG Zhi-feng, BAI Yue-long, SHI Li-kai. The method and apparatus for preparing the semisolid rheo-slurry or billets: CN101618438A [P]. 2008–01–06. (in Chinese)
- [8] ZHANG Zhi-feng, XU Jun, CHEN Xing-run. Numerical simulation on semi-solid metal slurry preparation by A-EMS [J]. Materials Science Forum, 2010, 654–656: 1492–1495.
- [9] TANG Meng-ou, XU Jun, ZHANG Zhi-feng, BAI Yue-long. New method of direct chill casting of Al-6Si-3Cu-Mg semisolid billet by annulus electromagnetic stirring [J]. Transactions of Nonferrous Metals Society of China, 2010, 20(9): 1591–1596.
- [10] ZHANG H T, NAGAUMI H, ZUO Y B, CUI J Z. Coupled modeling of electromagnetic field, fluid flow, heat transfer and solidification during low frequency electromagnetic casting of 7XXX aluminum alloys. Part 1: Development of a mathematical model and comparison with experimental results [J]. Materials Science and Engineering A, 2007, 448(1–2): 189–203.
- [11] DUGNOL ALVAREZ B, FERNANDEZ MARTINEZ J L, GARZON MARTIN M L, CALLEJA QUINTANA J M. Mathematical modelling of the process of continuous casting of aluminium and its alloys [J]. Finite Elements in Analysis and Design, 1999, 33(1): 43–59.
- [12] BELAHOUEL M, BOUMEDMED R. Numerical simulation of solidification processes in continuous casting. Influence of casting speed [J]. International Review of mechanical Engineering, 2008, 2(1): 159–162.
- [13] WECKMAN D C, NIESSEN P. A numerical simulation of the D.C. continuous casting process including nucleate boiling heat transfer [J]. Metallurgical and Materials Transactions B, 1982, 13(4): 593–602.
- [14] SPENCER D, FLEMINGS M C. Rheological behavior of Sn-15%Pb in the crystallization range [J]. Metallurgical Transactions, 1972, 3(7): 1925–1932.
- [15] FLEMINGS M C. Behavior of metal alloys in the semisolid state [J]. Metallurgical Transactions A, 1991, 22(5): 957–981.

## 环缝结构对电磁连铸流场和温度场的影响

汤孟欧, 徐 骏, 张志峰, 白月龙

北京有色金属研究总院, 北京 100088

**摘 要:** 建立描述环缝式电磁连铸 A357 铝合金圆坯过程的数学模型, 采用有限元法求解电磁场, 采用有限体积法求解流场和温度场, 并对电磁场和温度场的计算结果进行实验验证, 分析环缝宽度、环缝位置和芯棒长度等结构参数对环缝式电磁连铸过程流场、温度场和凝固过程的影响。结果表明: 环缝宽度越小, 液穴中的温度梯度越小, 温度场越均匀; 随着芯棒长度的增加, 由于芯棒的错位液穴内的循环流减小, 温度梯度变大; 当环缝位于铸坯边沿时, 液穴中的温度梯度降低明显。

**关键词:** 电磁搅拌; 连铸; 耦合场; 环缝

(Edited by YANG Hua)